

# Hot and cold bubbles in M87

Christian R. Kaiser\*

*Department of Physics & Astronomy, University of Southampton, Southampton SO17 1BJ*

31 October 2018

## ABSTRACT

The X-ray data obtained with *XMM-Newton* is used to investigate the complex structure of the gas in the atmosphere of the Virgo cluster around M87. We construct a simple model for the temperature and density distribution. This model implies that the cumulative mass of the cluster gas is a power-law of its entropy index,  $kTn^{-2/3}$ , similar to the Hydra cluster. This supports the idea that such power-laws are a direct consequence of gas cooling in a gravitational potential. In the cluster atmosphere hot bubbles of gas injected by the AGN are rising buoyantly. We estimate the age of these structures from the synchrotron radio data and find that this ‘radiative age’ is consistent with the estimated dynamical timescale. However, this requires a spatial separation of the relativistic particles from the magnetic field. The age estimates suggest an activity cycle of the AGN in M87 of roughly  $10^8$  years. We show that the largest radio structures are consistent with being the remnants of buoyant bubbles injected by the AGN during an even earlier activity cycle. The wakes behind the currently rising hot bubbles uplift cold gas from the cluster centre. Using a simple model for the trajectory of the cold gas, we demonstrate that the observations by *XMM-Newton* of a mix of hot and cold gas in the cluster atmosphere in the vicinity of the radio structure can be explained in this scenario. This may also explain the ridges of enhanced X-ray emission from cold gas observed with *CHANDRA*.

**Key words:** cooling flows – clusters: individual: Virgo – galaxies: active – galaxies: individual: M87

## 1 INTRODUCTION

The X-ray data from the *CHANDRA* and *XMM-Newton* satellites have shown that the hot gas in galaxy clusters is not the multiphase gas envisaged in the standard cooling flow picture (for a review see Böhringer et al., 2002). The gas is clearly radiatively cooling but this does not lead to distributed mass dropout and the cooling must be interrupted at least occasionally by heating from non-gravitational energy sources (e.g. Voit & Bryan, 2001; Voigt et al., 2002; Kaiser & Binney, 2003). Recently, heating by the outflows from AGN in the cluster centres has attracted much attention (e.g. Reynolds et al., 2001; Ruszkowski & Begelman, 2002; Brüggén & Kaiser, 2002; Basson & Alexander, 2003). This process is complicated and the exact details are still subject to debate. It is therefore of crucial importance to investigate clusters containing AGN in as much detail as possible. Because of its proximity, M87 in the Virgo cluster is the ideal target for such studies.

X-ray data from *ROSAT* (Böhringer et al., 1995) in combination with low frequency radio observations (Owen et al., 2000, hereafter OEK00) have already shown that the outflow from the AGN in M87 significantly influences the gas in the Virgo cluster (Böhringer et al., 1995; Harris et al., 1999). In this system it has been suggested that hot, rarefied plasma bubbles in-

jected by the AGN are rising buoyantly in the cluster atmosphere, uplifting in their wake colder material from the cluster centre (Churazov et al., 2001, hereafter CBK01). More recent observations with *XMM-Newton* (Böhringer et al., 2001; Belsole et al., 2001; Molendi & Pizzolato, 2001; Molendi & Gastaldello, 2001; Gastaldello & Molendi, 2002; Matsushita et al., 2002, hereafter MBF02; Molendi, 2002, hereafter M02) and with *CHANDRA* (Young et al., 2002, hereafter YWM02) confirm the presence of a mixture of hot and cold gas in the regions influenced by the AGN outflow (MBF02, M02, YMW02). Thus not radiative cooling but the activity of the AGN creates a multi-phase medium in the cluster atmosphere: (i) A relatively hot component representing the bulk of the gas which would be present even without the AGN, (ii) even hotter bubbles injected by the AGN and buoyantly rising in the gravitational potential of the cluster and (iii) cold bubbles uplifted from the cluster centre in the wake of the hot bubbles.

In this paper we show that the X-ray and radio observations of M87 and the surrounding Virgo cluster are consistent with an atmosphere containing all three of the above components. We start by relating the idea of hot and cold bubbles to the radio and X-ray observations in Section 2. In Section 3 we will use the X-ray data to construct a model for the temperature and density distribution of the cluster atmosphere, component (i). We also show that the cumulative mass of this gas is a power-law of its entropy index as suggested for cooling cluster atmospheres by Kaiser & Binney

\* email: crk@astro.soton.ac.uk

(2003). Section 4 derives an upper limit for the age of the buoyant hot bubbles, component (ii), from their radio synchrotron emission and shows that this is consistent with their estimated dynamical age. We show that this requires the spatial separation of the relativistic electrons from the magnetic field. In Section 5 we develop a simple model to determine the trajectory of cold gas clouds, component (iii), uplifted by the rise of the hot bubbles. The results from this model are consistent with the *XMM-Newton* data. Finally, we summarise our conclusions in Section 6. Throughout we assume the distance of the Virgo cluster to be 15.9 Mpc (Tonry, 1991).

## 2 MORPHOLOGY

Radio maps of the central regions of the Virgo cluster show three distinct features. Following YWM02 we refer to these as the bright ‘inner’ radio lobes extending to about 30 arcsec ( $\sim 2.5$  kpc) from the cluster centre, the ‘intermediate’ radio structures at roughly 3 arcmin ( $\sim 15$  kpc) and the ‘outer’ radio halos reaching out to 8 arcmin ( $\sim 40$  kpc). The inner radio lobes are the well-known, bright structures in the immediate surroundings of the radio jet and the radio core. The intermediate radio structure to the east of the cluster centre shows a distinct torus or ‘ear’-shape structure connected to the inner lobes by a bridge of radio emission. The entire structure resembles the ‘mushroom’ cloud caused by the buoyant rise of a bubble of hot gas in the gravitational potential of the cluster (CBK01). To the west and south-west of the centre the morphology is less clear, but OEK00 argue that the observations indicate a torus similar to that on the eastern side which is somewhat disrupted. In the following study of the hot buoyant bubbles and colder bubbles uplifted in their wake, we concentrate mainly on this intermediate structure. Finally, the outer halos give the appearance of two almost circular regions with diameters of 4 arcmin ( $\sim 40$  kpc) superimposed on the inner radio structures.

The high resolution X-ray *CHANDRA* observations of YWM02 reveal ridges of enhanced emission following the intermediate radio structures remarkably well. The X-ray ridge on the eastern side extends to at least the centre of the radio torus, roughly 3.3 arcmin from the cluster centre. In the south-west, the X-ray ridge appears to extend somewhat further. YWM02 also show that the temperature of the gas in the region of the X-ray ridges is significantly lower than in their surroundings. They demonstrate that the X-ray spectrum of the ridges extending to 3.3 arcmin is better fitted by a model assuming a mixture of hot and cold gas compared to a single temperature model. Based on the lower resolution *XMM-NEWTON* observations, M02 argues that two temperature models provide a better fit to the data out to about 6 arcmin from the cluster centre.

In this paper we interpret the torus structures observed in the radio on intermediate scales as buoyant bubbles containing hot gas. Bubbles of cold gas from the cluster centre are uplifted in the wake of the hot bubbles. These cold bubbles could be responsible for the observed ridges of enhanced X-ray emission and will lead to a mixture of hot and cold gas in the vicinity of the intermediate radio structure.

## 3 FITTING THE CLUSTER ATMOSPHERE

For our investigation of the properties and evolution of the hot and cold bubbles of gas in the surroundings of M87 in the Virgo cluster, we require a model for the cluster atmosphere. The best data for this

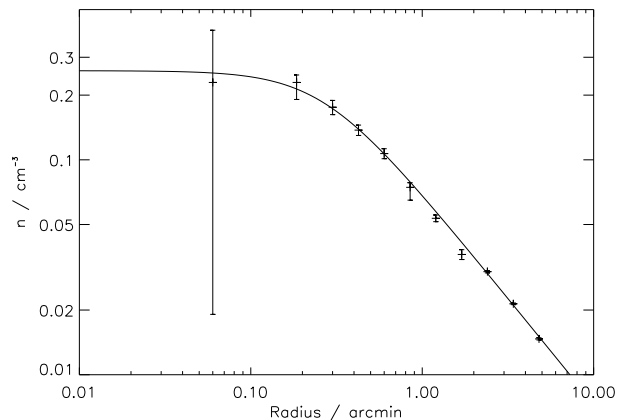


**Figure 1.** Model fit to the density distribution of the atmosphere of the Virgo cluster. Data points are taken from MBF02. The solid line shows the  $\beta$ -model used here.

purpose is provided by the X-ray observations of the Virgo cluster obtained with *XMM-Newton*. Temperature profiles of the cluster atmosphere can be obtained by fitting single or double temperature MEKAL models to the data (MBF02, M02). Using spectral deprojection techniques, the density distribution of the gas can also be determined (MBF02). Both methods require the averaging of the observational data over concentric annuli around the cluster centre. Thus the temperature and density are given only at a limited number of radii (see data points in Figure 1).

In this paper we are mainly interested in the properties of the cluster atmosphere at radii  $< 6$  arcmin. Out to this radius the *XMM-NEWTON* observations suggest the presence of a mixture of hot and cold gas in the cluster atmosphere (M02). We assume that the cluster gas within this radius has been affected by the AGN activity. Within this region we fit the density distribution with a  $\beta$ -model,

$$n = \frac{n_0}{\left[1 + (r/a_0)^2\right]^{1.5\beta}}, \quad (1)$$

where  $r$  is the radius from the cluster centre. The free parameters  $\beta$ ,  $a_0$  and  $n_0$  are determined by comparison of the model with the data. We use the density points given by MBF02 which we convert from electron density to gas density using  $n = 21/11n_e$ .

Figure 1 shows a comparison of the data with the  $\beta$ -model for the density with  $n_0 = 0.26 \text{ cm}^{-3}$ ,  $a_0 = 0.27$  arcmin and  $\beta = 0.33$ . We did not attempt a formal fit of the model to the data as this would require calculating the X-ray emission predicted by the model, folding this with the telescope response and then analysing the model emission in the same way as the observations. The  $\beta$ -model shown here is in reasonable agreement with the data and our conclusions are not affected by the exact choice of the model parameters. MBF02 also fit the density points with two rather than a single  $\beta$ -model. We prefer the simpler single  $\beta$ -model here as it provides a reasonable description of the data within 6 arcmin of the cluster centre.

The entropy index of the cluster gas is given by  $\sigma = kTn^{-2/3}$ . Using the density and temperature values of MBF02 we calculate  $\sigma$  at 11 radii inside 6 arcmin from the cluster centre. Integrating the  $\beta$ -model for the density distribution, we can also determine the mass of the gas inside these radii. Figure 2 shows the resulting plot of the cumulative gas mass,  $M(< \sigma)$  as function of  $\sigma$ . In the Hydra

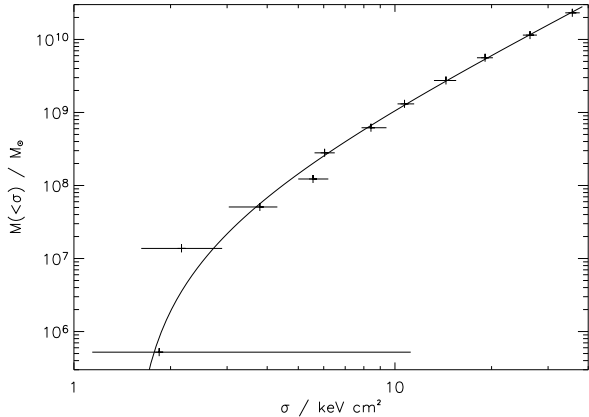


**Figure 2.** Plot of the cumulative mass of gas with entropy index below  $\sigma$  as function of  $\sigma$ . Data points are derived from the density and temperature data given by MBF02. The error bars for  $\sigma$  result from the uncertainty in the density and temperature measurements. The solid line shows the best fit power-law of the form given in equation (2).

cluster  $M(< \sigma)$  is observed to follow a simple power-law relation with  $\sigma$  of the form (Kaiser & Binney, 2003)

$$M(< \sigma) = A (\sigma - \sigma_0)^\epsilon, \quad (2)$$

with

$$A = \frac{M(< \sigma_{\max})}{(\sigma_{\max} - \sigma_0)^\epsilon}. \quad (3)$$

Here  $\sigma_0$  is the lowest value of the entropy index of gas at the centre of the cluster and  $\sigma_{\max}$  is the largest entropy index of gas contributing to the total gas mass  $M(< \sigma_{\max})$ . The solid line in Figure 2 shows the power-law described in equation (2) providing the best fit to the data when taking into account the uncertainties in the entropy index of the gas,  $\sigma$ . We conclude that equation (2) allows a good approximation of the data within 6 arcmin of the cluster centre for  $\epsilon = 2.3$ ,  $\sigma_0 = 1.5 \text{ keV cm}^2$ ,  $\sigma_{\max} = 40 \text{ keV cm}^2$  and  $M(< \sigma_{\max}) = 2.5 \times 10^{10} M_\odot$ . Kaiser & Binney (2003) pointed out that, once established, radiative cooling of the cluster gas with the cooling function presented in Figure 9-9 of Binney & Tremaine (1987) preserves the power-law form of  $M(< \sigma)$  and may indeed create a power-law distribution in the first place. The observations of the hot atmosphere in the Virgo cluster is consistent with this view.

Combining equations (1) and (2) allows us to express the entropy index as a function of radius,

$$(\sigma - \sigma_0)^\epsilon = \frac{4\pi\mu m_p n_0 a_0^3}{A} \int_0^{r/a_0} \frac{x^2}{(1+x^2)^{3/2\beta}} dx, \quad (4)$$

where  $m_p$  is the mass of a proton and  $\mu$  is the mean relative atomic weight of the cluster gas. The temperature of the cluster gas is then given by  $kT = \sigma n^{2/3}$ . Figure 3 compares the prediction from the models with the measurements. Although this is not a model fit, the agreement is reasonably good. For ideal gas conditions, we can also find an expression for the gas pressure of the cluster gas,  $p = \sigma n^{5/3}$ .

Assuming that the hot cluster atmosphere is in hydrostatic equilibrium within the gravitational potential of the dark matter halo of the Virgo cluster, the gravitational acceleration is given by

$$g = -\frac{1}{\mu m_p n} \frac{dp}{dr}. \quad (5)$$

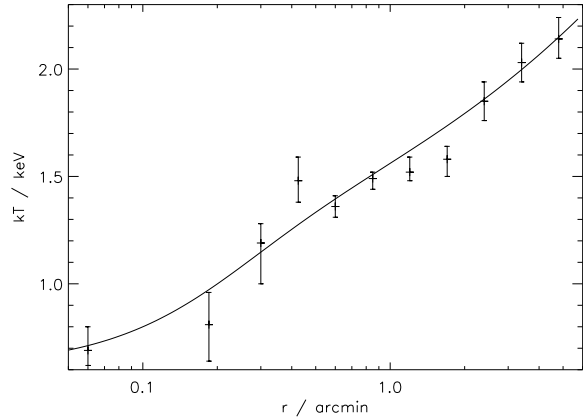


**Figure 3.** Comparison of the gas temperature (solid line) resulting from the combination of the  $\beta$ -model of the gas density distribution (Figure 1) and the power-law relation between cumulative gas mass and entropy index (Figure 2) with the observations of MBF02 (crosses with error bars).

It is now straightforward to show that

$$g = n^{2/3} r \left\{ \frac{5\beta\sigma}{\mu m_p a_0^2 \left[ 1 + \left( \frac{r}{a_0} \right)^2 \right]} - \frac{4\pi}{\epsilon A} (\sigma - \sigma_0)^{1-\epsilon} r n \right\}. \quad (6)$$

## 4 HOT BUBBLES FROM THE AGN

### 4.1 Intermediate radio structures

We adopt the idea of CBK01 that the intermediate radio structure resembling a torus observed to lie eastwards of the currently active AGN in M87 (OEK00) is a bubble of rarefied plasma rising buoyantly in the colder cluster atmosphere. The situation on the western side of the AGN is less clear, but a similar buoyant structure may exist on this side as well.

The ear-like radio structure on the eastern side extends over roughly 3.2 arcmin ( $\sim 15 \text{ kpc}$ ) in a north-south direction. Identifying this structure with a buoyant bubble containing gas significantly hotter than the surrounding material implies that we may expect to detect a depression of the X-ray surface brightness in this region. Such ‘holes’ have been detected in a number of clusters and strongly support the recent ideas of heating of the cluster gas by AGN outflows. Using the model for the gas distribution in the Virgo cluster derived in the previous section, we can estimate the expected depression of the X-ray surface brightness from the buoyant bubble at this location. For a completely evacuated spherical bubble with diameter 3.2 arcmin at a distance of 3.3 arcmin from the cluster centre, the X-ray surface brightness would decrease by roughly 30% for a line of sight through the centre of the bubble compared to a cluster without such a bubble. Such a strong depression is not detected in the *CHANDRA* data. However, various effects will make the detection of any suppression of the X-ray surface brightness due to a buoyant bubble difficult. Firstly, because of its buoyant motion, the hot bubble displaces and compresses cluster gas leading to the formation of a dense shell around the bubble. Assuming the shell thickness to be 1/10 of the bubble diameter the enhanced emission of the dense shell roughly compensates for the emission deficit caused by the bubble. Because of the strong de-

pendence of the X-ray emissivity on gas density, the bubble would show up as an X-ray *enhancement* if the shell was thinner. Secondly, the buoyant bubble is almost certainly not spherical because fluid instabilities will deform it into a torus (e.g. CBK01). The observed radio structure suggests such a toroidal geometry. The length of our line of sight through the bubble will therefore always be shorter than the diameter of the torus leading to a reduced effect of the bubble on the X-ray surface brightness. Finally, there is clear evidence for cold gas in the X-ray map at the location of the centre of the radio torus. We will argue further on that this cold material is uplifted from the cluster centre by the hot bubble. Its enhanced X-ray emission complicates the detection of any X-ray depression by the hot bubble. In all other clusters where holes in the X-ray surface brightness are observed, the bubbles appear spherical rather than torus-shaped. Also, in these clusters the bubbles may not be buoyantly rising anymore which implies the absence of a dense shell around the bubble. In fact, a close inspection of the *CHANDRA* map shows very slight depressions of the X-ray surface brightness immediately north and south of the torus centre (A.J. Young, private communication). In general the deviations from perfect spherical symmetry of the X-ray surface brightness of the gas in the Virgo cluster makes it very difficult to detect X-ray depressions in this highly complex region.

The detection of an X-ray hole at the location of the radio ‘ear’-structure would show beyond doubt the existence of a buoyant bubble filled with hot gas at this position. Its absence means that we cannot prove the existence of the postulated bubble. However, the morphology of the radio structure in combination with the work of CBK01 strongly suggests that a hot, buoyant bubble causes the ‘ear’-shaped structure to the east of the cluster centre.

CBK01 showed that a buoyant bubble will quickly reach its terminal rise velocity,  $v_t$ , defined by the balance of the buoyant and drag forces acting on the bubble. In the case of M87  $v_t \sim 400 \text{ km s}^{-1}$  and thus the position of the bubble as a function of time is simply  $r = v_t t$ . We cannot determine how projection changes the apparent distance of the bubble from the cluster centre in the radio observations of OEK00. The direction of the buoyant rise of the hot bubbles is determined by the properties of the large-scale distribution of gas in the cluster atmosphere rather than the direction of the currently active jet inside the inner radio structure. If the line connecting the eastern bubble with the cluster centre makes an angle  $\theta$  with our line of sight, then the bubble is currently located about  $15.4(\sin\theta)^{-1}$  kpc from the cluster centre. If the bubble started its journey at the cluster centre, then its age must be  $t_c = 3.8 \times 10^7 (\sin\theta)^{-1}$  years. To demonstrate the influence of the viewing angle  $\theta$  on our results, we consider the cases  $\theta = 90^\circ$  and  $\theta = 30^\circ$ . The latter case corresponds to a doubling of the unprojected distance of the bubble from the cluster centre and thus a bubble age of  $t_c = 7.6 \times 10^7$  years.

The bubble is observed to emit synchrotron radio emission of frequencies at least up to 10.55 GHz (Rottmann et al., 1996). As CBK01 showed, this is hard to reconcile with the usual assumption that the bubble is filled uniformly with relativistic particles and a magnetic field tangled on scales smaller than the bubble’s size. Only if the magnetic field is much lower than its equipartition value can the electrons barely survive their constant energy losses for long enough to explain the observations.

The assumption of a uniform distribution for the magnetic field in the radio structures caused by AGN may well be too simplistic (e.g. Eilek et al., 1997, and references therein). OEK00 point out that the entire large-scale radio structure of M87 shows filamentary substructure that may very well indicate an inhomoge-

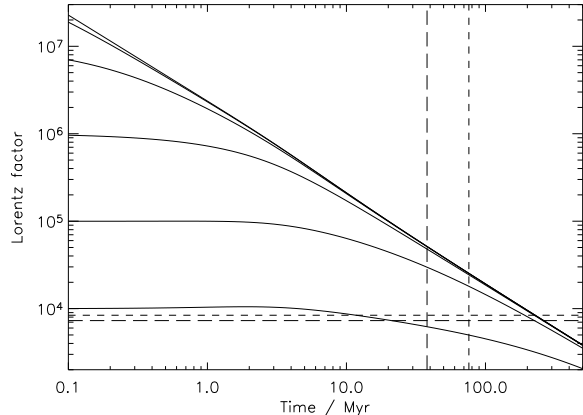


**Figure 4.** Evolution of the Lorentz factor for electrons inside the buoyant bubble. Solid lines show evolutionary paths for electrons with initial Lorentz factors equal to (from top to bottom)  $10^9$ ,  $10^8$ , ...,  $10^4$ . The dashed, horizontal lines show the Lorentz factor of electrons currently required in the bubble to explain the radio observations (Long-dashed:  $\theta = 90^\circ$ , short-dashed:  $\theta = 30^\circ$ ). The dashed, vertical lines show the estimated current age of the bubble for the two viewing angles considered here.

neous magnetic field in this region. Sophisticated models of the synchrotron emission from plasmas threaded by an inhomogeneous magnetic field have been developed in the literature (e.g. Tribble, 1993, 1994; Eilek et al., 1997). Here we only consider the limiting case in which the radio structure is made up of regions filled with a tangled magnetic field in pressure equilibrium with regions devoid of any magnetic field but containing relativistic particles. For simplicity we will also assume that the electrons do only diffuse into the areas containing the magnetic field but once inside do not diffuse out again. Thus, while in the field-free regions, the electrons are subject to energy losses only due to the adiabatic expansion of the buoyant bubble and due to inverse Compton scattering of the Cosmic Microwave Background (CMB) radiation. For the Lorentz factor of a relativistic electron,  $\gamma$ , we can therefore write

$$\frac{d\gamma}{dt} = -\frac{\gamma}{3V} \frac{dV}{dt} - \frac{4\sigma_T}{3m_e c} u_c \gamma^2, \quad (7)$$

where  $V$  is the volume of the bubble containing the relativistic electrons,  $\sigma_T$  is the Thomson cross-section,  $m_e$  is the electron mass and  $u_c$  is the energy density of the CMB. Because of the adiabatic expansion of the bubble during its rise, we can replace  $V$  with the pressure of the bubble which must be equal to that of the cluster atmosphere at the location of the bubble,

$$\frac{d\gamma}{dt} = \frac{\gamma}{3\Gamma p} \frac{dp}{dt} - \frac{4\sigma_T}{3m_e c} u_c \gamma^2, \quad (8)$$

where  $\Gamma$  is the ratio of specific heats of the bubble material. In the following we will assume  $\Gamma = 4/3$ . Using the results of Section 3, it is straightforward to numerically solve this differential equation.

The bubble regions containing the magnetic field are in pressure equilibrium with the cluster atmosphere. For  $r = 15$  kpc, the current position of the bubble if  $\theta = 90^\circ$ , this implies that  $B = 70 \mu\text{G}$ . For  $\theta = 30^\circ$ , we find  $r = 30$  kpc and  $B = 54 \mu\text{G}$ . Relativistic electrons diffusing into this magnetic field will mainly radiate at a frequency  $\nu \sim \gamma^2 eB / (2\pi m_e c)$ , where  $e$  is the elementary charge. Therefore the eastern bubble observed at 10.55 GHz in M87 must currently contain electrons with a Lorentz factor  $\gamma \geq 7300$  for  $\theta = 90^\circ$  and  $\gamma \geq 8400$  for  $\theta = 30^\circ$ .

Figure 4 shows the results of solving Equation (8) for the pressure profile derived in Section 3. We assume that electrons are injected into the bubble at time  $t = 0$  and then passively lose energy during the rise of the bubble. To explain the observations the electrons must clearly be injected with Lorentz factors of several  $10^4$ . It is also interesting to note that even for initially  $\gamma \rightarrow \infty$  the lifetime of the electrons is limited to about  $2 \times 10^8$  years. This is mainly caused by the inverse Compton scattering losses. If we neglect the adiabatic term in Equation (8) and set  $\gamma \rightarrow \infty$  at  $t = 0$ , we can solve directly for  $\gamma$  yielding

$$\gamma = \frac{3m_e c}{4\sigma_T u_e t}, \quad (9)$$

which gives  $t_{\max} = 3 \times 10^8$  years for  $\gamma = 8000$ .

From these considerations it becomes clear that the observed radio emission can be explained in terms of a single injection of relativistic electrons into the buoyant bubble. However, this almost certainly requires a non-uniform magnetic field structure. In the case of the eastern torus the maximum lifetime of the relativistic electrons is consistent with the age of the structure estimated from dynamical considerations. Even for a viewing angle to the path of the hot bubble of  $\theta = 30^\circ$  to our line of sight, an initial injection of relativistic electrons into the buoyant bubble is consistent with the radio observations. However, the relativistic electrons could easily diffuse into the cluster atmosphere if they are not bound to the bubble by at least a weak magnetic field. The field needed to prevent diffusion is very weak but would of course further shorten the lifetimes of the electrons.

The alternative to the scenario sketched above is that relativistic particles are constantly re-accelerated in the buoyant bubble. This would require the presence of shocks and/or strong turbulence. Such sites of ongoing particle acceleration should in principle be very conspicuous as bright spots in the radio images. The observed filaments could of course mark regions of particle acceleration. However, they are not very much brighter than their surroundings and they are more naturally interpreted as local enhancements of the magnetic field. In any case, shocks or strong turbulence would require a supersonic or at least chaotic fluid flow inside the buoyant bubble. This is hard to reconcile with the subsonic and comparatively smooth buoyant rise of the bubble in the cluster atmosphere suggested for the formation of the torus and circular structures.

## 4.2 Outer Radio structures

All the arguments above also apply to the relativistic electrons in the almost circular outer radio structures enveloping the tori on intermediate scales discussed so far. CBK01 interpreted the outer structures as buoyant bubbles that were released from the AGN even earlier than the torus structures and have reached their iso-entropy surfaces. If this interpretation is correct, the outer radio structures cannot be older than a few  $10^8$  years or otherwise we would not detect them. This implies that the AGN in M87 must have a duty cycle of roughly  $10^8$  years or shorter.

At the iso-entropy surface the bubbles stop rising and start spreading. Thus the circular emission regions should be thin (CBK01). As they must be roughly in pressure equilibrium with their surroundings, the location of these bubbles at their iso-entropy surface implies that their mass density must be equal to that of the surrounding cluster medium. The density of the relativistic electrons responsible for the observed radio synchrotron emission is orders of magnitude lower than that of the cluster gas. Therefore

the spreading bubbles must contain a significant amount of thermal material mixed with the relativistic particles and the magnetic field. Obviously we cannot decide whether this thermal material was present in the bubbles at the time their buoyant rise started or whether it was mixed in during the rise itself. In any case, the thermal electrons embedded in the magnetic field could lead to Faraday rotation and thus depolarisation of the radio synchrotron emission.

Rottmann et al. (1996) find the polarisation of the synchrotron emission at 10.55 GHz from the outer radio structures to exceed 70% of the total flux. This is close to the theoretical upper limit for the polarisation and indicates that the synchrotron radiation suffers very little depolarisation. We use the simple models of Cioffi & Jones (1980) to calculate the expected internal depolarisation due to the thermal electrons inside the spreading bubbles. For a conservative estimate we assume that the circular outer radio structures are at the same distance ( $\sim 15$  kpc) from the cluster centre as the intermediate tori. The  $\beta$ -model fit for the density of the cluster gas derived in section 3 then implies an electron density of  $0.01 \text{ cm}^{-3}$  inside the spreading bubbles. We also assume that the magnetic field inside the bubbles is comparable to that in the intermediate torus structures ( $70 \mu\text{G}$ ). If we allow a maximum reduction of 5% of the fraction of polarised flux, the thickness of the bubbles along our line of sight must be less than 1 kpc. Although we cannot place any other constraints on this dimension of the bubbles, the picture of a spreading bubble is probably consistent with a ratio of bubble thickness and bubble diameter in the plane of spreading of 1/40. In case the spreading bubbles are further away from the cluster centre, then both the electron density and the strength of the magnetic field are probably lower than assumed here. This leads to a higher upper limit on the thickness of the spreading bubbles. Finally, it should be noted that high degrees of polarisation do not necessarily imply the absence of thermal electrons in the synchrotron emission region. If the structure of the magnetic field is more complex than in the simple models used here, then large amounts of thermal material can be present without significant depolarisation taking place (Laing, 1984).

## 5 COLD BUBBLES LIFTED BY HOT BUBBLES

Simulating the buoyant rise of a hot bubble from the AGN, CBK01 found that cold material from the cluster centre was lifted to larger distances from the cluster centre in the wake of the hot bubble. Recently, MBF02 and M02 noted that the X-ray observations of M87 obtained with *XMM-Newton* strongly suggest the presence of a mixture of hot and cold plasma in the region influenced by the buoyant bubble. Here we argue that the cold component of this mixture can be identified with bubbles of cold gas uplifted from the cluster centre in the wake of a buoyant, hot bubble. The cold bubbles may also form the ridges of enhanced X-ray emission detected in the high resolution maps obtained with *CHANDRA* (YWM02).

The exact details of the trajectory of a bubble of cold gas dragged along by the rise of a hot bubble are complicated and their investigation require numerical simulations. Here we develop a very simple model for the motion of the cold bubbles in the cluster atmosphere. We assume that the passage of the hot bubble accelerates the cold bubble instantaneously to a fraction  $f \leq 1$  of the terminal rise velocity of the hot bubble,  $v_t$ . Thus the cold bubble moves outward but is decelerated because of a buoyant force,

$$F_b = -V(\rho_a - \rho_b)g, \quad (10)$$

acting on it. Here,  $V$  is the volume of the cold bubble,  $\rho_b$  and  $\rho_a$  are

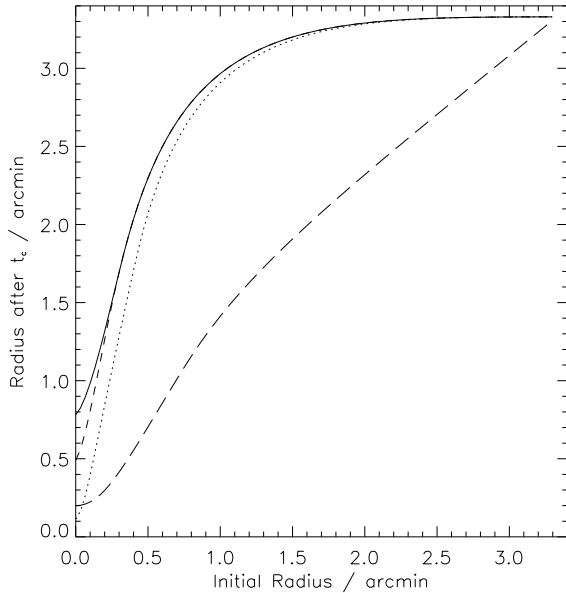


**Figure 5.** The position of an uplifted cold cloud at time  $t_c$  after the hot bubble started rising from the cluster centre. Solid line: Angle of bubble motion to line of sight  $\theta = 90^\circ$  (this implies  $t_c = 3.8 \times 10^7$  years), initial radius of uplifted bubbles  $R_s = 50$  pc, initial rise velocity of cold bubbles as fraction of terminal velocity of hot bubble  $f = 1$ . Long-dashed line: Same as solid line but  $f = 0.25$ . Short-dashed line: Same as solid line but  $R_s = 500$  pc. Dotted line: Same as solid line but  $\theta = 30^\circ$ , in this case  $t_c = 7.6 \times 10^7$  years.

the mass density of the cold bubble and of the cluster atmosphere in the vicinity of the bubble respectively and  $g$  is the gravitational acceleration exerted by the dark matter halo (see Equation 5). The cold bubble is surrounded by cluster gas which would normally exert a drag force on the bubble. However, as all the material in the wake of the hot bubble is moving with roughly the same velocity, because it is subject to the same gravitational acceleration, we can neglect the drag force here. This situation changes once the cold bubble comes to rest and starts sinking back towards the cluster centre under the influence of the buoyant force. Now its surroundings are at rest and will exert a drag force

$$F_d = \frac{1}{2} C S v^2 \rho_a, \quad (11)$$

where  $S$  is the surface area of the bubble on which the drag force acts and  $v$  is its velocity. The drag coefficient  $C$  is of order unity and we set it to 0.75 which was found for the hot, buoyant bubble in the simulations of CBK01. The equation of motion for the cold bubble is therefore

$$\frac{d^2 r}{dt^2} = g \left( 1 - \frac{\rho_a}{\rho_b} \right) + \frac{3}{4} \frac{C}{R} \left( \frac{dr}{dt} \right)^2 \frac{\rho_a}{\rho_b}, \quad (12)$$

where we have assumed that the cold bubble is a sphere with radius  $R$ . During its rise and subsequent fall, the cold cloud will be in pressure equilibrium with the cluster atmosphere. The radiative cooling time of the cloud material is long compared to the dynamical timescales considered here and so the evolution of the cloud will be adiabatic. The pressure equilibrium and the adiabatic behaviour allow us to self-consistently determine the radius,  $R$ , and other properties of the cold cloud.

Consider a bubble of gas located initially at a radius  $r_s$  from

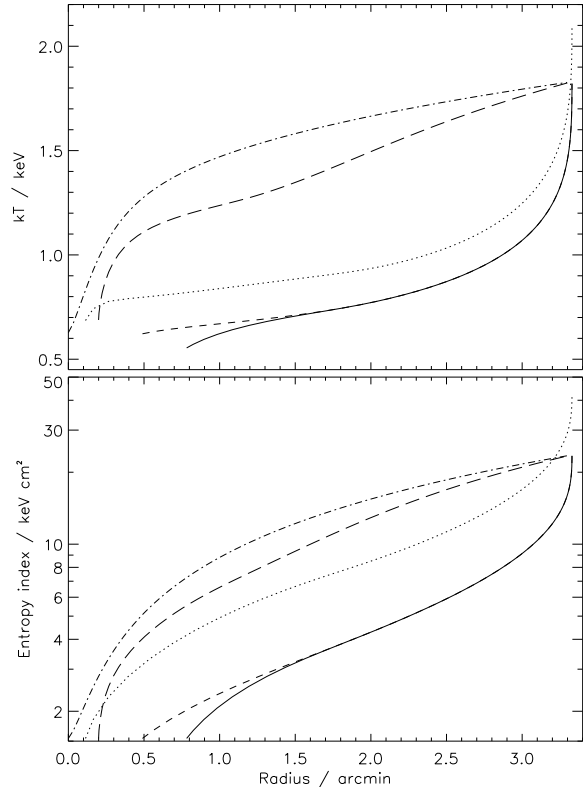


**Figure 6.** Temperature and entropy index distribution of the cold clouds as a function of radius at time  $t_c$  after the hot bubble started rising from the cluster centre. Line styles as in Figure 5. The dot-dashed line shows the temperature and entropy index distribution of the unperturbed cluster gas for  $\theta = 90^\circ$ .

the cluster centre. For this bubble we start the integration of Equation (12) at the time the hot bubble passes through  $r_s$ . At this point in time, the hot bubble accelerates the cold bubble instantaneously to  $f v_t$ . While the cold bubble is rising, we neglect the drag force. We set the initial radius of the cold bubbles to  $R_s$ . The position of the cold bubble at time  $t_c$  after the hot bubble started its rise in the cluster centre, i.e. the current time, is shown in Figure 5 as a function of  $r_s$ . The result depends somewhat on the angle to our line of sight  $\theta$  of the path of the cold bubbles in the wake of the hot bubble. However, projection reduces this effect because the longer rise time of the hot bubble compensates for the longer unprojected distances the cold bubbles have to travel. Maybe somewhat surprisingly the size of the uplifted, cold bubbles has a very limited effect on their final position. However, only the contribution of the drag force to equation (12) depends on the bubble size. All cold bubbles originally located outside a radius of about 0.3 arcmin from the cluster centre are still rising at time  $t_c$ . By construction, no drag force acts on these clouds and so their motion is independent of their size.

The results presented in Figure 5 depend crucially on the initial velocity of the cold clouds. If the buoyant hot cloud does not accelerate the cold clouds to a significant fraction of its own rise velocity, then the restructuring of the cluster atmosphere through uplift of cold clouds is not very significant. Even for a moderate reduction of their initial velocity ( $f = 0.25$ ), the cold clouds do not rise very far in the cluster before starting to fall back to their initial positions.

Initially we assume that the cold clouds are part of the clus-

ter gas at radius  $r_s$ , i.e. their temperature and density are given by our models of the cluster atmosphere discussed in Section 3. Using the adiabatic evolution of the cold clouds we can readily calculate the temperature and the entropy index of the cloud material at later times. In Figure 6 we show the distribution of the temperature and entropy index in the unprojected cluster atmosphere and for the uplifted cold clouds at the current time  $t_c$ . While rising, the cold clouds expand to adjust to the lower pressure further out in the cluster. Therefore they cool while their entropy index is of course constant. The pressure distribution in the cluster atmosphere leads to a virtually constant temperature of the cold clouds for most of the range in radius they occupy within the cluster. The exact value of this temperature depends on the projection angle  $\theta$ , but the flat temperature profile is preserved independent of the values of  $\theta$  or  $f$ . Again we find that only for a slower initial velocity of the cold clouds this result is significantly altered because the cold clouds do not rise very far within the cluster atmosphere. A constant temperature of the uplifted cold bubbles is consistent with the observational results of M02. Note also that for strong projection, i.e. small values of  $\theta$ , the temperature of the cold clouds located furthest away from the cluster centre naturally exceeds the temperature of the unperturbed gas of the unprojected cluster atmosphere. Deprojection would show that this material is located at larger radii where the temperature is higher than the projected image suggests.

The entropy index distribution of the cold bubbles is simply shifted and stretched in the direction of increasing radius compared with the unperturbed cluster gas. Again this is consistent with the findings of M02. Projection has a much stronger influence on the entropy index distribution compared to the temperature distribution. For small values of  $\theta$  we would expect a small difference between the entropy index of the unperturbed cluster gas compared to that of the cold bubbles. M02 find that for a given radius the entropy index of the cold gas component in the Virgo cluster is roughly a factor 3 lower than that of the hot component. A qualitative comparison with Figure 6 shows that this indicates  $\theta \sim 90^\circ$  for the cold bubbles uplifted by the hot bubble associated with the ‘intermediate’ radio structure in the Virgo cluster.

Note here that there is no *a priori* reason why observations of cold clouds uplifted by hot bubbles from AGN in other clusters should result in a similar constant temperature distribution. However, for the specific conditions of the cluster atmosphere in the Virgo cluster the observations of cold material associated with the radio structure are consistent with the uplift of cold clouds described here.

## 6 CONCLUSIONS

The excellent data on the hot, gaseous atmosphere of the Virgo cluster obtained with *XMM-Newton* allows us to accurately fit the temperature and density distribution of the cluster gas. Using these models we find that the cumulative mass of the cluster gas,  $M(< \sigma)$ , is a power-law function of the form presented in Equation (2) of the entropy index  $\sigma = kTn^{-2/3}$ . For the Virgo cluster we find  $\epsilon = 2.3$  and  $\sigma_0 = 1.5 \text{ keV cm}^2$ . The Virgo cluster is therefore the second cluster after the Hydra cluster for which such a power-law has been found. This supports the suggestion of Kaiser & Binney (2003) that these distributions arise naturally in cluster atmospheres under the influence of radiative cooling by bremsstrahlung.

We revisit the idea that the torus structure seen to the east of the currently active AGN in M87 is caused by the buoyant rise of a hot bubble injected by an earlier activity cycle of the AGN. If

there was a single injection of relativistic electrons responsible for the synchrotron radio emission into the bubble at the time it started its buoyant rise, then the fact that it is still detectable at 10.55 GHz (Rottmann et al., 1996) implies a maximum age of  $3 \times 10^8$  years for this structure. However, this requires that the relativistic electrons are separated from the magnetic field for most of the time. The dynamical age is of order  $5 \times 10^7$  years and is therefore consistent with the ‘radiative age’ above. This result does not depend on projection effects.

The upper limit for the age derived here also applies to the circular emission regions seen in the map of OEK00. If these are the remnants of buoyant bubbles from an even earlier activity cycle as suggested by CBK01, then the duty cycle of the AGN in M87 must be of order  $10^8$  years. From the observations we cannot rule out a process constantly re-accelerating relativistic particles in the radio structures. However, their appearance and their interpretation as slowly rising buoyant structures make such a process unlikely. We propose that the bubbles forming the circular emission regions have reached their iso-entropy surface in the cluster atmosphere. This implies that they contain significant amounts of thermal material mixed with the relativistic particles and magnetic field giving rise to the radio synchrotron emission. We show that this scenario is consistent with the high degree of polarisation of the observed radio emission if the circular emission regions are thin and therefore seen in projection.

The hot bubble drags in its wake colder material from the cluster centre further out. We develop a simple model for the trajectory of such cold clouds. From this model we calculate the entropy index and temperature structure of the cold material in the Virgo cluster. The temperature of the cold material should be roughly constant as a function of radius over a large range of radii. The entropy index distribution of the cluster atmosphere is shifted and stretched in the direction of larger radii for the cold material. Both results depend crucially on the initial velocity with which the cold bubbles start rising in the wake of the hot bubble. If this initial velocity is significantly lower than the rise velocity of the hot bubble, then no flat temperature profile is found. Projection effects do not alter the shape of the temperature or entropy index distributions. However, they determine the absolute values of these gas properties of the cold clouds at a given radius. Our findings do not depend significantly on the size of the cold bubbles.

A flat temperature profile and the entropy distribution are consistent with the temperature and entropy index distribution of the cold component in the cluster atmosphere derived directly from the X-ray data by M02. The flat temperature structure arises from the uplifting of material from a range of initial radii. This material naturally has a range of initial temperatures. The pressure distribution of the cluster atmosphere of Virgo then leads to the observed temperature distribution. We conclude that the mixture of hot and cold gas in the atmosphere of Virgo can be explained by the uplift of cold gas from the cluster centre by the buoyant hot bubbles injected by the AGN.

The Virgo cluster is probably the best studied cooling flow cluster containing an active AGN. The superb quality of the X-ray and radio data enable us to study the interaction of the AGN and the cluster gas in great detail. The results presented here suggest that further X-ray studies of other clusters containing AGN should reveal a power-law relation between the gas mass and the entropy index of the gas and a mixture of hot and cold gas in the regions influenced by the AGN activity.

**ACKNOWLEDGMENTS**

The author would like to thank Dr. A.J. Young and Dr. M. Hardcastle for useful discussions and the anonymous referee for many helpful comments.

**References**

- Basson J. F., Alexander P., 2003, *MNRAS*, 339, 353
- Belsole E., Sauvageot J. L., Böhringer H., Worrall D. M., Matsushita K., Mushotzky R. F., Sakelliou I., Molendi S., Ehle M., Kennea J., Stewart G., Vestrand W. T., 2001, *A&A*, 365, L188
- Binney J. J., Tremaine S., 1987, *Galactic Dynamics*. Princeton University Press
- Böhringer H., Belsole E., Kennea J., Matsushita K., Molendi S., Worrall D. M., Mushotzky R. F., Ehle M., Guainazzi M., Sakelliou I., Stewart G., Vestrand W. T., Santos S. D., 2001, *A&A*, 365, L181
- Böhringer H., Matsushita K., Churazov E., Ikebe Y., Chen Y., 2002, *A&A*, 382, 804
- Böhringer H., Nulsen P. E. J., Braun R., Fabian A. C., 1995, *MNRAS*, 274, L67
- Brüggen M., Kaiser C. R., 2002, *Nat.*, 418, 301
- Churazov E., Brüggen M., Kaiser C. R., Böhringer H., Forman W., 2001, *ApJ*, 554, 261, [CBK01]
- Cioffi D. F., Jones T. W., 1980, *AJ*, 85, 368
- Eilek J. A., Melrose D. B., Walker M. A., 1997, *ApJ*, 483, 282
- Gastaldello F., Molendi S., 2002, *ApJ*, 572, 160
- Harris D. E., Owen F., Biretta J. A., Junor W., 1999, in Böhringer H., Feretti L., Schuecker P., eds, *Diffuse Thermal and Relativistic Plasma in Galaxy Clusters MPE Report No. 271*, p. 111
- Kaiser C. R., Binney J. J., 2003, *MNRAS*, 338, 837
- Laing R. A., 1984, in Bridle A. H., Eilek J. A., eds, *Physics of energy transport in extragalactic radio sources*. NRAO: Greenbank, WV, p. 90
- Matsushita K., Belsole E., Finoguenov A., Böhringer H., 2002, *A&A*, 386, 77, [MBF02]
- Molendi S., 2002, *ApJ*, 580, 815, [M02]
- Molendi S., Gastaldello F., 2001, *A&A*, 375, L14
- Molendi S., Pizzolato F., 2001, *ApJ*, 560, 194
- Owen F. N., Eilek J. A., Kassim N. E., 2000, *ApJ*, 543, 611, [OEK00]
- Reynolds C. S., Heinz S., Begelman M. C., 2001, *ApJ*, 549, L179
- Rottmann H., Mack K., Klein U., Wielebinski R., 1996, *A&A*, 309, L19
- Ruszkowski M., Begelman M. C., 2002, *ApJ*, 581, 223
- Tonry J. L., 1991, *ApJ*, 373, L1
- Tribble P. C., 1993, *MNRAS*, 261, 57
- Tribble P. C., 1994, *MNRAS*, 269, 110
- Voigt L. M., Schmidt R. W., Fabian A. C., Allen S. W., Johnstone R. M., 2002, *MNRAS*, 335, L7
- Voit G. M., Bryan G. L., 2001, *Nat.*, 414, 425
- Young A. J., Wilson A. S., Mundell C. G., 2002, *ApJ*, 579, 560, [YWM02]